

Docetaxel Conjugate Nanoparticles That Target α -Smooth Muscle Actin-Expressing Stromal Cells Suppress Breast Cancer Metastasis

Mami Murakami^{1,2}, Mark J. Ernsting^{1,2}, Elijus Undzys¹, Nathan Holwell¹, Warren D. Foltz³, and Shyh-Dar Li^{1,4}

Abstract

Docetaxel-conjugate nanoparticles, known as Cellax, were synthesized by covalently conjugating docetaxel and polyethylene glycol to acetylated carboxymethylcellulose via ester linkages, yielding a polymeric conjugate that self-assembled into 120 nm particles suitable for intravenous administration. In 4T1 and MDA-MB-231 orthotopic breast tumor models, Cellax therapy reduced α -smooth muscle actin (α -SMA) content by 82% and 70%, respectively, whereas native docetaxel and nab-paclitaxel (albumin-paclitaxel nanoparticle, Abraxane) exerted no significant antistromal activity. In Cellax-treated mice, tumor perfusion was increased by approximately 70-fold (FITC-lectin binding), tumor vascular permeability was enhanced by more than 30% (dynamic contrast-enhanced magnetic resonance imaging), tumor matrix was decreased by 2.5-fold (immunohistochemistry), and tumor interstitial fluid pressure was suppressed by approximately 3-fold after Cellax therapy compared with the control, native docetaxel, and nab-paclitaxel groups. The antistromal effect of Cellax treatment corresponded to a significantly enhanced antimetastatic effect: lung nodules were reduced by 7- to 24-fold by Cellax treatment, whereas native docetaxel and nab-paclitaxel treatments were ineffective. Studies of the 4T1 tumor showed that more than 85% of the Cellax nanoparticles were delivered to the α -SMA+ stroma. Significant tumor stromal depletion occurred within 16 hours (~50% depletion) postinjection, and the α -SMA+ stroma population was almost undetectable (~3%) by 1 week. The 4T1 tumor epithelial cell population was not significantly reduced in the week after Cellax injection. These data suggest that Cellax targets tumor stroma and performs more efficaciously than docetaxel and nab-paclitaxel. *Cancer Res*; 73(15); 4862–71. ©2013 AACR.

Introduction

Breast cancer is a common malignancy and a leading cause of cancer-related death in women, with mortality largely attributable to metastatic spread to vital organs such as lung, liver, and bone (1–3). Advances in drug delivery have potential to improve therapy, and nanomedicine approaches exhibit particular promise (4–6). Nanoparticle therapies leverage the enhanced permeability and retention (EPR) effect: tumor vasculature is abnormally permeable compared with normal

vasculature, and as a result, nanoparticles can migrate selectively into tumor tissues (4). Nanoparticle therapy can increase the dose of chemotherapy to tumor tissue, and spare normal tissue from exposure (7). However, enhancing drug delivery to the tumor does not necessarily equate to improved bioavailability (8): the drug must be internalized by tumor cells, and ideally would target cells that are responsible for tumor spread.

The tumor microenvironment is an important contributor of tumor progression and response to treatment, and therefore it is important to develop novel therapies that target the microenvironment. Stromal cells play a vital role in tumor growth, angiogenesis, and progression (9). For example, fibroblasts are mesenchymal cells normally responsible for the construction, maintenance, and remodeling of connective tissues (10), but differentiate to activated cancer-associated fibroblasts (CAF) when exposed to paracrine signals released from malignant neoplasms. CAFs constitute the major population of tumor stroma. These cells are characterized by high α -smooth muscle actin (α -SMA) expression and excrete a panel of cytokines that act upon both stromal and tumor cells, amplifying both cell numbers and enhancing the malignant phenotype (11). In addition, cytokines stimulate stromal and tumor cells to excrete matrix metalloproteinases (MMP), enzymes that degrade extracellular matrix (ECM) and enable tumor and stromal cell migration into healthy tissue and into

Authors' Affiliations: ¹Drug Delivery and Formulation, Drug Discovery Program, Ontario Institute for Cancer Research; ²Faculty of Engineering and Architectural Science, Ryerson University; ³Spatio-Temporal Targeting and Amplification of Radiation Response (STTARR) Program, Princess Margaret Hospitals Radiation Medicine Program; and ⁴Leslie Dan Faculty of Pharmacy, University of Toronto, Toronto, Ontario, Canada

Note: Supplementary data for this article are available at Cancer Research Online (<http://cancerres.aacrjournals.org/>).

M. Murakami and M.J. Ernsting contributed equally to this work.

Corresponding Author: Shyh-Dar Li, Ontario Institute for Cancer Research, 101 College Street, MaRS Centre South Tower, Suite 800, Toronto, Ontario M5G 0A3, Canada. Phone: 647-260-7994; Fax: 416-673-6664; E-mail: sli@oicr.on.ca

doi: 10.1158/0008-5472.CAN-13-0062

©2013 American Association for Cancer Research.

the systemic circulation (11, 12). Further, these stromal cells deposit ECM in remodeled tissues, creating a supportive scaffold for tumor cell proliferation. Therefore, normalization or elimination of the activated or reactive stromal compartment is a potential approach to cancer control (9). Approaches to treating the stroma include targeting of VEGF (angiogenesis), MMPs (matrix remodeling), and suppression of the hedgehog pathway, but clinical success has been limited, as human tumors tend to become resistant to drugs that block these pathways (13).

We have recently developed a docetaxel conjugate of polyethylene glycol (PEG)ylated acetylcarmethyl-cellulose, known as Cellax. The Cellax polymeric conjugate exhibits a high drug loading (~37 wt% docetaxel), condenses into well-defined approximately 120 nm nanoparticles in saline, releases drug at a controlled rate in serum (~5%/day), and exhibits good stability in saline at 4°C (> 6 months; refs. 14, 15). Compared with native docetaxel (the commonly used Tween80 detergent formulation, Taxotere) and nab-paclitaxel (an albumin nanoformulation of paclitaxel, Abraxane), Cellax exhibits a 5 and 20 times longer serum half life and 39 and 37 times higher plasma area under the curve (AUC_{0-240h}), respectively (16). Cellax also shows selective accumulation in tumors with 5- and 10-fold increased uptake compared with native docetaxel and nab-paclitaxel, respectively (15, 16). Here, we report the therapeutic effects on the mouse-model breast tumor microenvironment after treatment with native docetaxel, nab-paclitaxel, and Cellax, and compare their antistromal and antimetastatic activities. Comparisons of tumor perfusion and permeability (histology and magnetic resonance imaging), and interstitial fluid pressure (IFP) are carried out as functional metrics that relate stromal depletion to efficacy outcomes. We also report the intratumoral uptake and efficacy of Cellax against α -SMA stroma and tumor epithelial populations.

Materials and Methods

Materials

Abraxane (nab-paclitaxel) and Taxotere (native docetaxel) were purchased from the University Health Network pharmacy. Cellax polymer and particles (including DiI-containing particles) were prepared as described previously (14–17). Additional reagents are described in Supplementary Material. Cellax particle size and zeta potential were measured on a Malvern NanoZS instrument, and docetaxel content was measured by a UV method (14, 15). The Cellax particles were sterile filtered through a 0.22 μ m filter and tested for endotoxin using the Limulus amoebocyte lysate (LAL) turbidity assay and sterility was determined using the agar plate assay (Nanotechnology Characterization Lab).

Cell culture and animals

Mouse 4T1 and human MDA-MB-231 breast cancer cell lines were obtained from the American Type Culture Collection. Female Balb/c mice (4T1) and female NOD-SCID mice (MDA-MB-231) were purchased from Jackson Laboratories. All protocols were approved by the Animal Care Committee of the University Health Network.

Efficacy in orthotopic breast tumor models

Efficacy analysis of Cellax, native docetaxel, and nab-paclitaxel was conducted in 2 orthotopic mouse models of breast cancer (4T1 and MDA-MB-231). Doses of Cellax, native docetaxel, and nab-paclitaxel were administered at their maximum-tolerated doses (MTD), determined previously (15, 16). 4T1 model: The MTD of Cellax (170 mg docetaxel/kg), native docetaxel (40 mg/kg), or nab-paclitaxel (170 mg/kg) was administered via tail vein injection 4 days postinoculation of the 4T1 cells into the breast fat pads (1×10^6 cells/injection, $n = 10$ mice per group) of female Balb/c mice (i.e., when tumors reached 5–7 mm in diameter). Six days later, the primary tumors were resected and fixed for histologic examination, and on day 13, the mice received a second round of therapy. On day 20, all mice were sacrificed, and lung tissues were harvested and fixed for histology analysis. MDA-MB-231 model: MDA-MB-231 cells were inoculated into the breast fat pad (2×10^6 cells/injection, $n = 10$ mice per group) of female NOD-SCID mice: tumors required 4 weeks to become established and attain a diameter of 7 to 8 mm. Mice were treated by intravenous injection at the MTD of Cellax (150 mg docetaxel/kg), native docetaxel (5 mg/kg), or nab-paclitaxel (50 mg/kg), and 1 week later were treated a second time. Primary tumors were resected 3 weeks after the second treatment. The mice were monitored for additional 70 days, at which time they were sacrificed, and lungs were harvested and fixed for histologic analysis.

Before resection of the primary tumors, the mice were evaluated with a series of additional tests, as described below.

Interstitial fluid pressure

IFP in the 4T1 and MDA-MB-231 tumors (see above) was measured using an established wick-in-needle technique (18, 19) 1 day before tumor resection. Mice were lightly anesthetized by isoflurane, and 2 to 3 measurements per tumor were made on 8 to 10 mice per group. IFP was calculated as the pressure change (ΔP) from baseline to average maximum pressure measured more than 10 seconds.

Perfusion analysis

Mice-bearing orthotopic tumors ($n = 5$) received an intravenous injection of fluorescein isothiocyanate (FITC)-lectin 1 hour before primary tumor resection. Tumor sections stained for CD31 were imaged by confocal microscopy (6 images per tumor, Olympus Fluoview, $\times 20$) and colocalization analysis of CD31 and FITC-lectin signal was conducted in ImagePro. CD31-positive blood vessels colocalized with FITC-lectin were identified as perfused blood vessels.

Dynamic contrast-enhanced magnetic resonance imaging

In the 4T1 efficacy study described above, the vascular perfusion and permeability of tumor tissue was measured just before tumor resection by Dynamic contrast-enhanced magnetic resonance imaging (DCE-MRI; ref. 20). Refer to Supplementary Material for a detailed protocol description. Contrast enhancement curves for rim and core tumor regions of 4T1 tumors were segmented and fitted to the Modified Tofts model

to quantify K_{trans} (influx volume transfer constant from blood to extravascular extracellular space/minute; ref. 21).

Tissue analysis

Tumor sections were stained for α -SMA with FITC and CD31 with Cy3 (refer to Supplementary Material for immunohistochemical methods). Selected slides were stained with hematoxylin and eosin (H&E) or Masson Trichrome. Fluorescently labeled images were generated on an Olympus FluoView confocal microscope at $\times 20$ magnification [Advanced Optical Microscopy Facility (AOMF)], and images were quantitatively analyzed on ImagePro Plus (Media Cybernetics). H&E or Masson Trichrome slides were scanned on a ScanScope XT microscope. Analyses were conducted on 5 tumors per group, with 5 to 6 fields of view per tumor. Tumor burden in the lungs of mice were calculated using Tissue Studio (Definiens Health Image Intelligence). Data from these analyses are expressed as % total area.

Tumor uptake of fluorescently labeled Cellax in 4T1 tumors

To facilitate a detailed analysis of Cellax distribution in 4T1 tumors, a larger tumor size was developed: when tumor diameter reached approximately 8 mm, the mice were treated with a single intravenous injection of DiI-labeled Cellax (200 μ L, 100 μ g DiI/mL content). One day later, the tumors were harvested, fixed, and prepared for α -SMA immunohistochemical staining (FITC label). Fluorescent images were scanned on a TissueScope (Huron Technologies), and colocalization analysis of α -SMA+ cells and Cellax-DiI was conducted using Definiens software.

Intratumoral efficacy

In a protocol similar to the 4T1 efficacy study, we prepared a 4T1 orthotopic breast tumor model, treated the mice with Cellax, and sacrificed the mice at selected time points posttherapy to analyze the response of the tumor and stromal cell populations more than 1 week posttherapy. When tumors reached approximately 8 mm in diameter, Cellax (170 mg docetaxel/kg) was injected into the tail veins of the mice. At selected times posttherapy (6, 16, 24, 72, and 168 hours), tumors were harvested and stained with H&E or for α -SMA (FITC; $n = 4$ samples per group). Fluorescent images were scanned on a TissueScope, and analysis of α -SMA+ cells, viable tumor epithelial (H&E) and nonviable areas (H&E) were conducted in Definiens software.

Cellax toxicology

We have previously compared the toxicity of native docetaxel, nab-paclitaxel, and Cellax by monitoring body weight and neutrophil count (16). Here, we studied Cellax safety using panels of hematology and blood chemistry, and tissue histology. Balb/c mice ($n = 5$) were dosed once weekly for 3 cycles with Cellax (170 mg docetaxel/kg). Blood and serum samples were collected for analysis (Toronto Centre for Phenogenomics) at baseline and 7 days after the 1st, 2nd, and 3rd doses. Further blood samples were collected at 2, 3, and 4 weeks post final dose. A full serology panel was only conducted at

baseline and the final 2 measurements, to minimize blood sampling volumes. Major organs from mice at 3 and 4 weeks post final dose were harvested, fixed in formalin, processed to produce H&E slides, and were graded by a veterinary pathologist at the Toronto Centre for Phenogenomics.

Statistical analysis

All data are expressed as mean \pm SD. Statistical analysis was conducted with the 2-tailed unpaired *t* test for 2-group comparison or one-way ANOVA, followed by Tukey multiple comparison test by using GraphPad Prism (for 3 or more groups). A difference with $P < 0.05$ was considered to be statistically significant.

Results

Cellax nanoparticle characterization

Cellax nanoparticle (Supplementary Fig. S1) characterization confirmed data from previous reports (14–17): particles were $121.5 \text{ nm} \pm 0.9 \text{ nm}$, a value that was stable at 10, 100, and 1,000 times dilution in saline. Particles exhibited a zeta potential of $-8.1 \pm 0.9 \text{ mV}$ (neutral), and tested negative for endotoxin or microbial contamination.

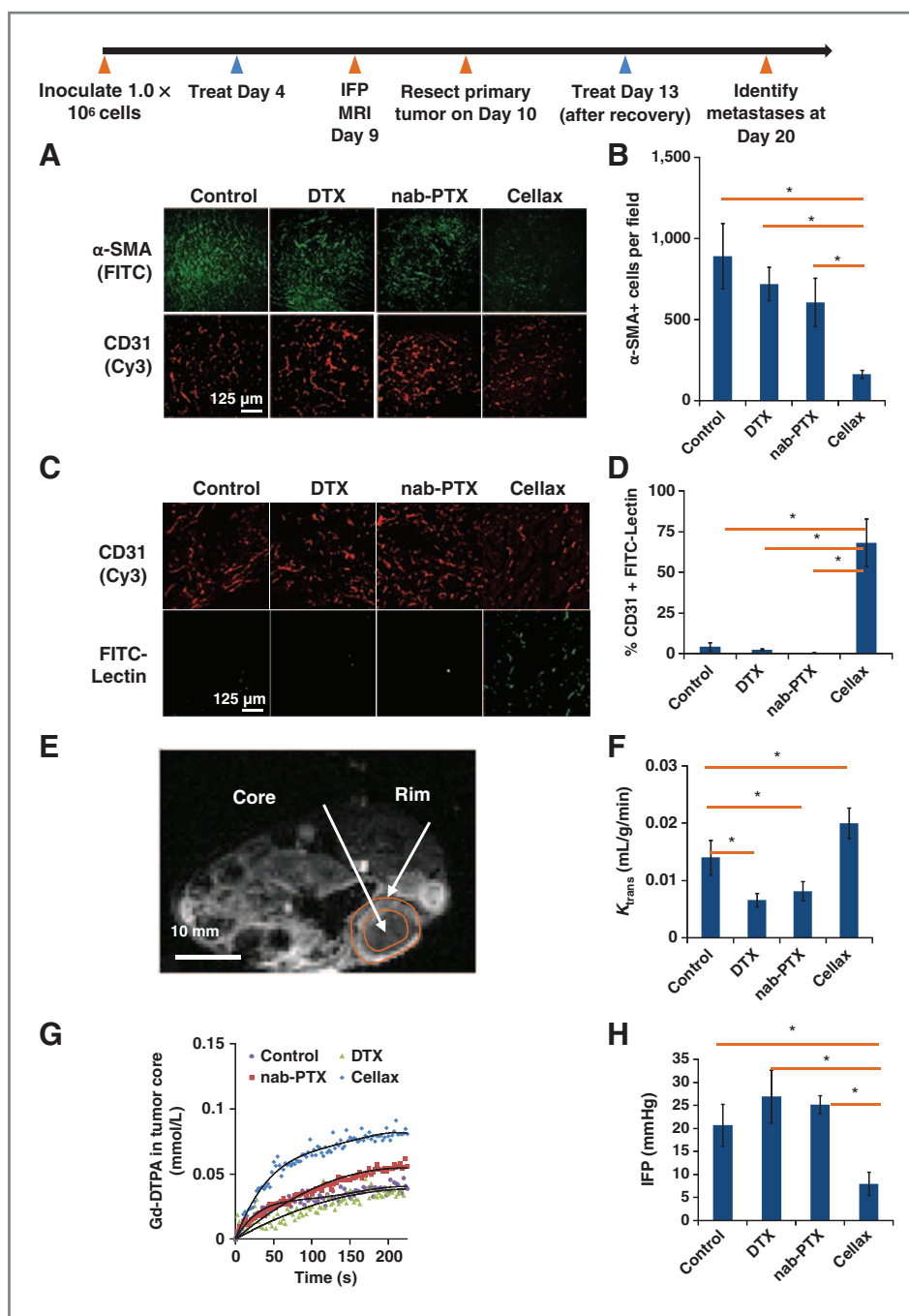
Cellax depletes α -SMA+ stromal cells in the tumor, increases vascular perfusion, and reduces metastases

Histologic analysis of 4T1 tumors resected 3 days after a single treatment (Fig. 1A), established that Cellax treatment induced a significant ($P < 0.05$) 82% reduction in α -SMA content (Fig. 1B), compared with nonsignificant reductions in tumors treated with native docetaxel and nab-paclitaxel. The density of blood vessels (Fig. 1A) did not vary significantly among treatment groups.

Cellax treatment induced a significant ($P < 0.05$) increase in blood vessel perfusion in 4T1 tumors, determined by histology analysis of FITC-lectin-labeled-treated tumors (Fig. 1C). In Cellax-treated mice, tumor blood vessels were better perfused (68%) compared with vessels from control-, native docetaxel-, and nab-paclitaxel-treated mice (0.4%–4.4%; Fig. 1D). DCE-MRI analysis of treated 4T1 tumors likewise indicated that the vascular permeability of the 4T1 tumors was improved. Post-injection of the Gd-DTPA probe, perfusion of the tumor rim was apparent and measurable in each treatment group (representative example in Fig. 1E), with no significant differences in the K_{trans} values (average K_{trans} across groups was $0.080 \pm 0.003 \text{ mL/g/min}$; Fig. 1F). The core of each tumor was less perfused ($0.014 \pm 0.003 \text{ mL/g/min}$ in the control mice). A significant increase ($P < 0.05$) in perfusion was measured in the core of Cellax-treated tumors ($0.020 \pm 0.002 \text{ mL/g/min}$, Fig. 1G), whereas decreases in perfusion were measured in native docetaxel- and nab-paclitaxel-treated tumors (0.006 ± 0.001 and $0.008 \pm 0.002 \text{ mL/g/min}$, respectively). K_{trans} was measured from the slope of the curves in Fig. 1G, but it is also worth noting that the maximum concentration of the Gd-DTPA in Cellax-treated tumors was approximately 2-fold higher compared with the control-, native docetaxel-, or nab-paclitaxel-treated mice.

α -SMA+ stromal cells exhibit a contractile phenotype, which contributes to vascular collapse and increased IFP

Figure 1. Therapeutic effects of native docetaxel (DTX), nab-paclitaxel (nab-PTX), and Cellax on the 4T1 orthotopic breast tumor. Balb/c mice were inoculated with 4T1 cells orthotopically to the mammary fat pad and were treated as depicted in the experimental schedule. Ten mice per group were inoculated. For histology and image analyses, 5 tumors per treatment group and 5 to 6 fields of view per image were collected and analyzed. **A**, primary tumor sections were stained for CD31 (blood vessels) and α -SMA (stromal cells), and were imaged by confocal microscopy at $\times 20$ magnification. **B**, quantification of α -SMA depletion was conducted in ImagePro software. Significant ($P < 0.05$) reductions in α -SMA were measured in Cellax-treated tumors. **C**, primary tumor sections from mice treated with FITC-lectin were sectioned and stained for CD31. **D**, colocalization of CD31 and FITC signal in ImagePro plus analysis showed that Cellax-treated tumors were perfused more than the other groups. **E**, DCE-MRI analysis of the primary tumor; Gd-DTPA contrast (white) is especially evident at the rim of tumors. **F**, analysis of the MRI showed that the core of Cellax-treated tumors was significantly more permeable. **G**, the MRI data showed that the maximum concentration of Gd-DTPA contrast in tumor cores was the highest in Cellax-treated tumors. **H**, tumor IFP was significantly reduced in the Cellax-treated tumors, an effect linked to reduced stroma and increased perfusion. *, $P < 0.05$.



(11, 22): given the reduction in α -SMA+ stromal cells and the observation of increased perfusion, we evaluated the effect of taxane therapies on IFP (Fig. 1H). IFP was reduced by 2.6-fold by Cellax treatment compared with control, whereas native docetaxel and nab-paclitaxel treatment had no significant effect on tumor pressure.

A significant ($P < 0.05$) reduction in the presentation of metastases was observed in the Cellax treatment group. All the control mice exhibited lung metastases (Fig. 2A), with incidence of presentation in bone (20%), spleen (30%), and primary

tumor recurrence (50%). The native docetaxel-treated mice presented with high incidence of lung metastases (90%), and incidence in bone (20%), spleen (10%), and recurrence of primary tumor (20%). The nab-paclitaxel-treated mice presented with a similar pattern of metastases: lung (86%), bone (0%), spleen (14%), and primary recurrence (29%). In contrast, only 40% of the Cellax-treated mice presented with visible tumor nodules on the lung, and no other visceral metastases were observed. Definiens image analysis of lung histology samples (Fig. 2B and C) indicated that Cellax reduced total

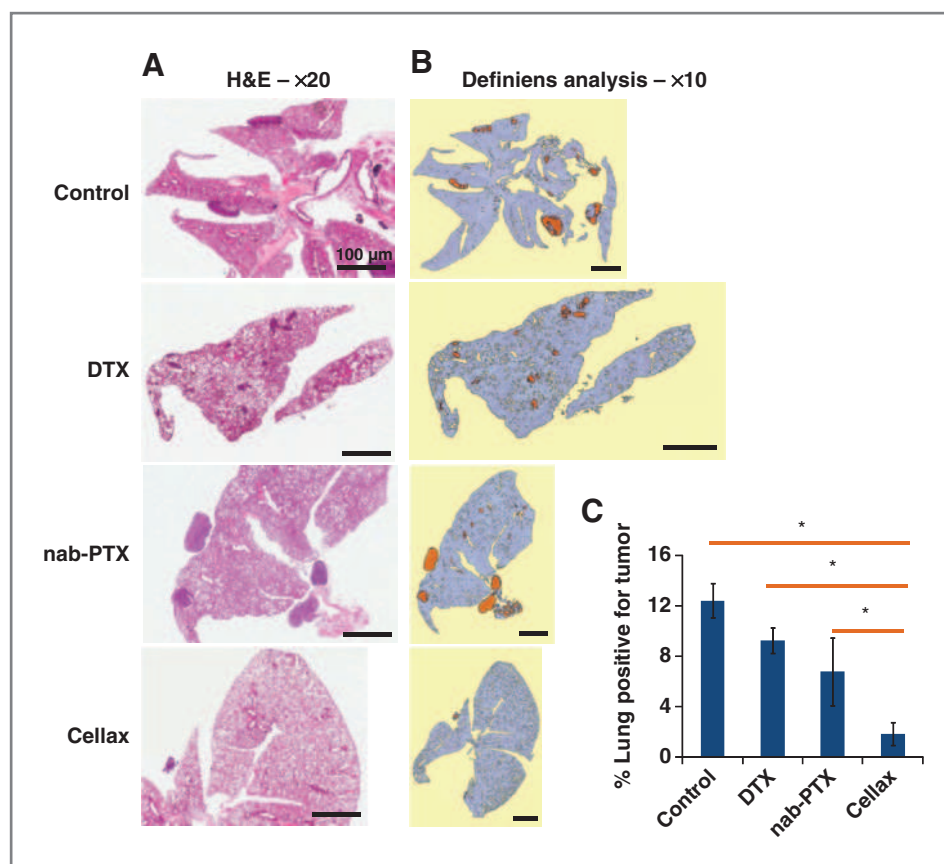


Figure 2. Antimetastatic effect of native docetaxel (DTX), nab-paclitaxel, and Cellax against the 4T1 breast tumor. Lung tissues from the Balb/c mice bearing 4T1 orthotopic breast tumors were analyzed for metastases ($n = 5$ per treatment group). H&E-stained sections (A) showed that the prevalence of tumors was visibly reduced in Cellax-treated mice. The tissue sections were analyzed in Definiens software (B) and the quantitative analysis (C) showed that tumor burden (orange) as a fraction of lung tissue (blue) was significantly reduced in the Cellax-treated mice. *, $P < 0.05$.

lung tumor burden by 6.7-fold compared with nonsignificant decreases in the native docetaxel and nab-paclitaxel treatment groups.

The effects of Cellax treatment observed in the 4T1 model translated to the MDA-MB-231 orthotopic breast model. Cellax-treated tumors exhibited a 70% reduction in total α -SMA content (Fig. 3A and B), compared with nonsignificant changes in the native docetaxel and nab-paclitaxel treatment groups. As the MDA-MB-231 tumors were slow growing, there was more evidence of matrix deposition: Cellax-treated tumors exhibited 63% less detectable matrix compared with control tumors (Fig. 3D), whereas no effect was observed in the native docetaxel- and nab-paclitaxel-treated tumors. Similar to the 4T1 model, IFP was reduced by 3.8-fold in the Cellax-treated tumors compared with the control (Fig. 3E), whereas native docetaxel and nab-paclitaxel treatment did not reduce the tumor IFP. As with the 4T1 model, the percentage of perfused blood vessels (Fig. 3F) was significantly increased in Cellax-treated MDA-MB-231 tumors (30% of blood vessels), compared with low FITC-lectin perfusion of control-, native docetaxel-, and nab-paclitaxel-treated tumors (Fig. 3G). As with the 4T1 model, there was no significant change in overall blood vessel density in any treatment group. Cellax treatment reduced lung tumor burden by 24.4-fold compared with control ($P < 0.05$), whereas native docetaxel treatment increased lung tumor burden by 1.7-fold ($P < 0.05$), and nab-paclitaxel treatment did not significantly reduce tumor burden (Fig 4).

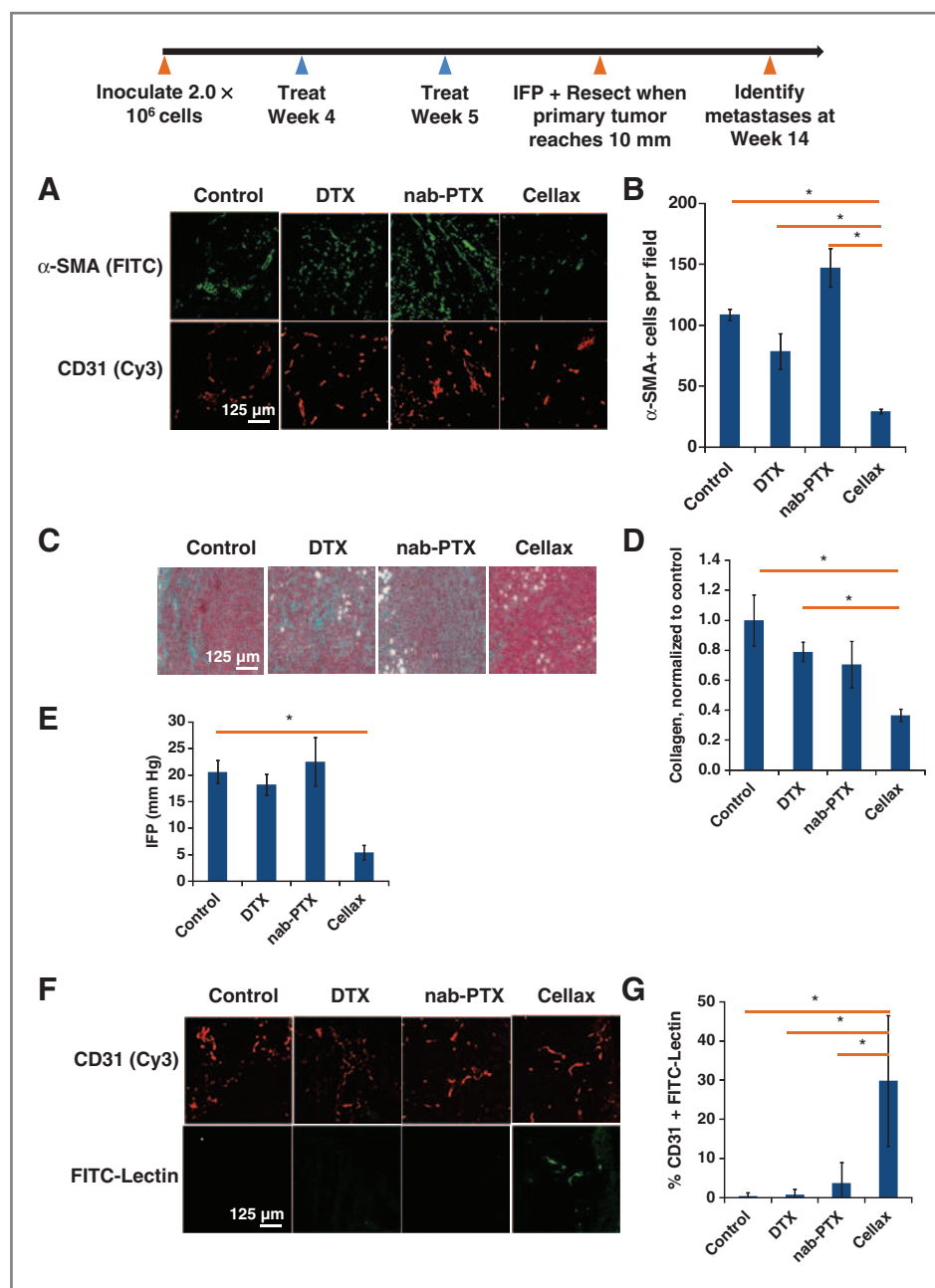
Cellax selectively associates with α -SMA+ stromal cells in the tumor

Cellax nanoparticles exhibited a strong interaction with stromal tissues, with more than 85% Cellax nanoparticles colocalized with α -SMA+ cells (Fig 5A). The α -SMA stromal depletion occurred rapidly after Cellax therapy: at 16 hours postinjection approximately 50% of the stroma was depleted, followed by a steady and continuous decline to an almost undetectable level ($\sim 3\%$) after 1 week (Fig 5B). The tumor cell population, on the other hand, was not significantly depleted 1 week post-Cellax injection. The nonviable tissue fraction in the tumor increased to 60% of tumor volume following Cellax treatment: as viable tumor cells were not significantly diminished in the first week (Fig 5B), and as α -SMA+ stromal cells were completely depleted, it follows that stromal cell depletion was the primary effect of Cellax therapy.

Cellax toxicology study

Cellax-treated mice did not exhibit the hallmark taxane toxicity of neutropenia, and despite significant clearance of Cellax in the liver (15), no evidence of alanine aminotransferase (ALT) or aspartate aminotransferase (AST) enzyme elevation was detected (Fig. 6 and Supplementary Table S1). The mice did not exhibit any loss of body weight. In histopathology analysis 1 week post the final dose (3 doses), mild lesions were detected in the liver (hypertrophic Kupffer cells) and the lung

Figure 3. Therapeutic effects of native docetaxel (DTX), nab-paclitaxel, and Cellax on the MDA-MB-231 orthotopic breast tumor. NOD-SCID mice were inoculated with MDA-MB-231 cells orthotopically to the mammary fat pad and were treated as depicted in the experimental schedule. Ten mice per group were inoculated. For histology and image analyses, 5 tumors per treatment group and 5 to 6 fields of view per image were collected and analyzed. A, primary tumor sections were stained for CD31 (blood vessels) and α -SMA (stromal cells), and were imaged by confocal microscopy at $\times 20$ magnification. B, quantification of α -SMA depletion was conducted in ImagePro software. Significant ($P < 0.05$) reductions in α -SMA were measured in the Cellax-treated tumors. C, tumor sections were stained with Masson Trichrome, and the blue color captured collagen content. Analysis of these images in ImagePro (D) showed that the Cellax-treated tumors contained less ECM. E, tumor IFP was significantly reduced in the Cellax-treated tumors. F, primary tumor sections from mice treated with FITC-lectin were sectioned and stained for CD31. G, colocalization of CD31 and FITC signal in ImagePro plus analysis showed that Cellax-treated tumors were more perfused than other treatment groups. *, $P < 0.05$.



(alveolar macrophage activation), both indicative of mild inflammation. These lesions became rare in samples analyzed 3 or 4 weeks post the final dose, indicating recovery. No other tissue abnormalities were observed.

Discussion

We have developed an enhanced drug delivery approach for docetaxel, and have previously shown that Cellax nanoparticles were effective in enhancing the pharmacokinetics, safety, and efficacy of docetaxel in subcutaneous and orthotopic mouse models of cancer (14–17). In this study, our analysis of Cellax efficacy in orthotopic breast models led to the discovery that Cellax interacts with α -SMA+ stromal cells,

leading to increased tumor permeability and perfusion, reduced IFP, and inhibition of metastases.

While enhancing drug delivery to the tumor tends to be a primary focus in the field, interaction of nanoparticles with tumor cells or supportive stromal cells is a determinant of drug bioavailability and antitumor activity (8). For example, while Doxil (liposomal doxorubicin) enhances tumor delivery of drug, the formulation exhibits a slow release profile with low bioavailability, and the efficacy is therefore not enhanced compared with native doxorubicin in human patients (8). We have reported that Cellax nanoparticles were readily internalized by cancer cell lines *in vitro* as well as by cells in solid tumors (15). Here, we report that Cellax interacted selectively

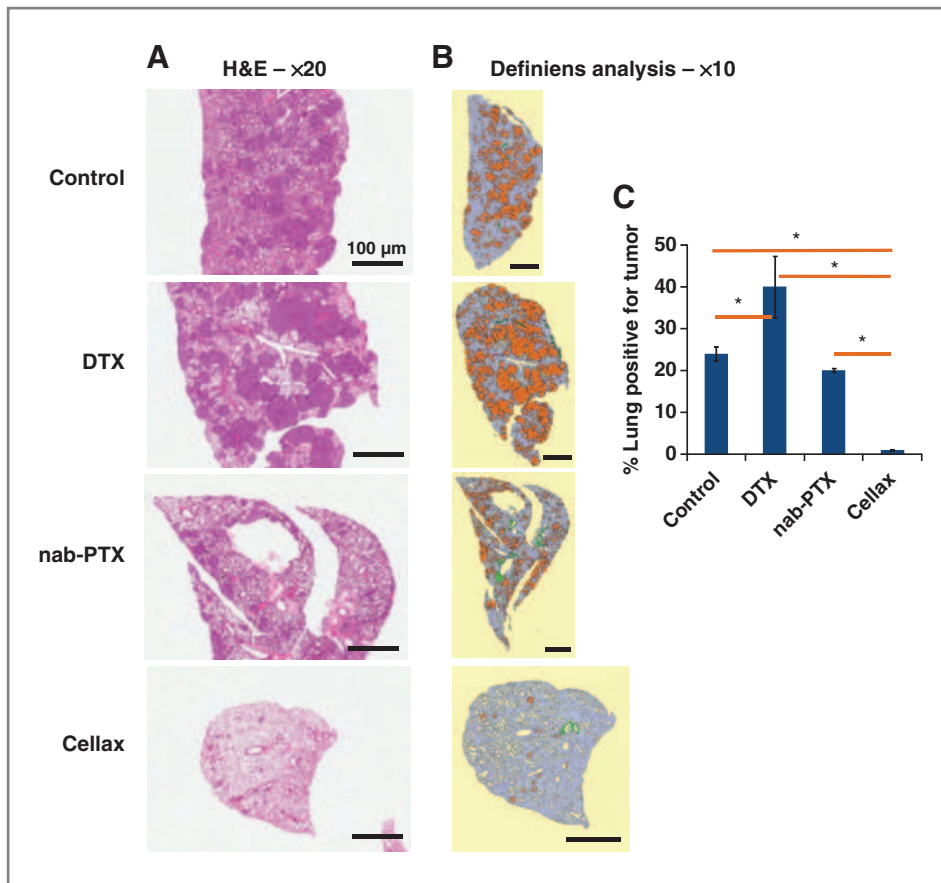


Figure 4. Antimetastatic effect of native docetaxel (DTX), nab-paclitaxel, and Cellax against the MDA-MB-231 breast tumor. Lung tissues from the NOD-SCID mice bearing MDA-MB-231 orthotopic breast tumors were analyzed for metastases ($n = 5$ per treatment group). H&E-stained sections (A) showed that the prevalence of tumors was visibly reduced in the Cellax-treated mice. The tissue sections ($n = 5$) were analyzed in Definiens software (B), and the quantitative analysis (C) showed that tumor burden (orange) as a fraction of lung tissue (blue) was significantly reduced in the Cellax-treated mice. Major blood vessels are depicted in green. The analysis also showed that native docetaxel treatment led to a significant increase in tumor-burden compared with the control mice. *, $P < 0.05$.

with tumor stromal cells *in vivo*, particularly the α -SMA+ population, which led to enhanced antitumor efficacy.

Tumor progression and metastasis are driven by interactions of tumor cells with stromal cells in the microenviron-

ment. These stromal cells are activated by growth factors such as transforming growth factor ($TGF\beta_1$), which are secreted from the tumor cells, and then express proinflammatory phenotypes typical of cells involved in the wound-healing

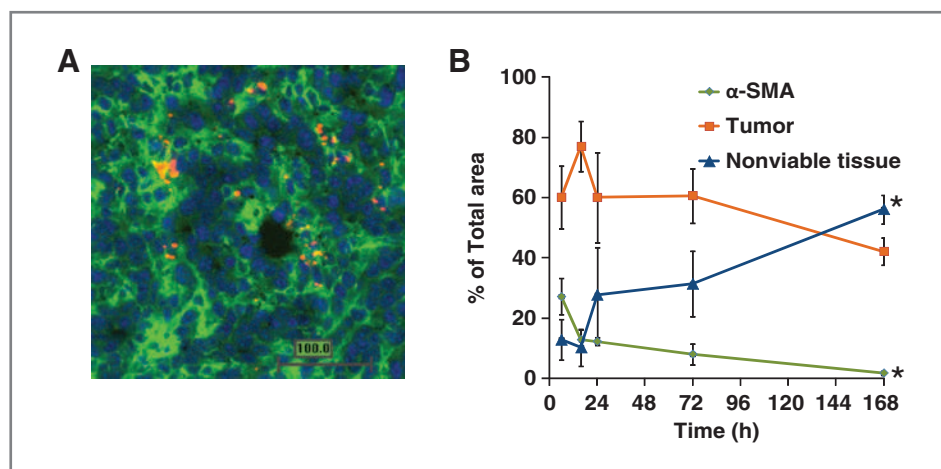


Figure 5. Intratumoral uptake and efficacy studies. A, Balb/c mice bearing 4T1 breast tumors ($n = 5$) were treated with fluorescently labeled Cellax particles (red), and the α -SMA cells were immunostained with FITC (green). DAPI stains nuclei (blue). Definiens image analysis of tumors for total area (defined by DAPI), α -SMA content (green), and Cellax-Dil (red) showed that 85% of the Cellax particles were associated with α -SMA+ cells. Cellax-treated 4T1 tumors were analyzed to quantify different cell populations in the tumors over a time course (B); subsequent to therapy, α -SMA content dropped rapidly more than 16 hours, followed by a steady decrease more than 168 hours. Tumor cells as a percentage of total tumor area did not undergo a significant decline in the 168 hours timeframe, whereas nonviable tissue increased significantly, suggesting that the decline of α -SMA+ cells is the primary therapeutic effect. *, $P < 0.05$.

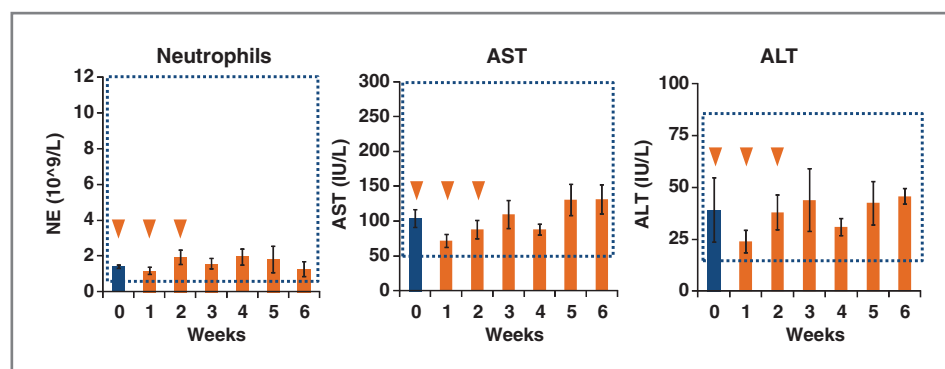


Figure 6. Safety profile of Cellax treatment. Balb/c mice were treated with Cellax once weekly for three cycles at 170 mg docetaxel/kg and were followed for 4 weeks after the third dose ($n = 5$ per treatment group). Orange triangles indicate when mice were dosed, and the blue bars indicate the baseline measurement. Parameters known to indicate taxane toxicity (neutrophils) or liver stress (AST and ALT enzymes) are emphasized. The hashed blue boxes indicate the normal range of values in healthy mice. Refer to Supplementary Table S1 for the full panel of analyses. No analyses were significantly different from baseline values.

cascade. Tumor-associated stromal cells actively release paracrine signals [stromal cell-derived factor 1 (SDF-1), hepatocyte growth factor (HGF), fibroblast growth factor (FGF) and many others], deposit ECM, remodel and contract tissues, and initiate angiogenesis (12, 23, 24). Indeed, reactive stromal tissues share many common features with granulation tissue (9). These processes, which are beneficial in normal wound healing, become pathologic when tumor cells are present (12, 24). The presence of a reactive stroma (desmoplasia) is implicated in treatment resistance, and high stromal activity is a biomarker for poor prognosis in people with cancer, and is associated with metastasis (12, 25). For example, women with breast cancer expressing high tumor α -SMA+ stroma (primary >50% stroma) exhibit a higher rate of relapse at 5 years than women whose tumors have low stroma (<50%; refs. 26, 27).

We selected 2 well-characterized orthotopic breast cancer models to study Cellax efficacy. 4T1 is a syngeneic and aggressively metastatic model: studies examining 4T1 metastases to lung and bone implicate stromal and ECM factors favoring metastasis (12, 24). MDA-MB-231 is a breast xenograft model that exhibits metastases to lung and bone, and lung metastasis is known to be influenced by stromal-related markers (28). In our efficacy analysis, significant reductions (7 and 24 times) in lung metastases in 4T1 and MDA-MB-231 models treated with Cellax (Figs. 2C and 4C) were accompanied by 82% and 70% reductions in α -SMA+ cells (Figs. 1B and 3B), respectively, prompting further investigation into the significance of the stromal depletion and impact on the tumor microenvironment. Cellax did not exhibit enhanced activity against the primary tumors in the mammary fat pad compared with native docetaxel and nab-paclitaxel as the tumor sizes were comparable during the therapies. However, tumors treated with Cellax were depleted of α -SMA+ stroma and the tumor metastases were significantly reduced, indicating the key role of α -SMA+ stroma in promoting tumor progression in these 2 tumor models.

Reduction in stroma was accompanied by increased tumor perfusion and reduced IFP. Deposition of matrix heavy in collagen, fibrinogen, and hyaluronan increases the rigidity of tumors, and combined with contractile activity and poor

fluid transport caused by abnormal permeability and perfusion, leads to increased IFP (11). A high IFP condition inhibits transport of oxygen and nutrients, promoting hypoxia and acidosis, conditions that in turn promote tumor cell aggression and metastatic spread. High IFP also limits drug transport; all these IFP-related factors contribute to tumor resistance (29, 30). Recent data suggests that reduction of stroma ameliorates the drug delivery barrier (31), and that depletion of stromal cells "primes" the tumor microenvironment for decreased IFP and enhanced drug penetration (32, 33). Cellax treatment reduced α -SMA+ stroma, reduced IFP by more than 50% in both the 4T1 and MDA-MB-231 tumors (Figs. 1H and 3E), and increased blood perfusion in the tumor core by more than 60 fold, as measured by FITC-lectin histology (Figs. 1D and 3G). The data in this study supports the hypothesis that reduced stroma is linked to reduced IFP and perfusion, and linked to a reduction in tumor growth and metastases.

Tumor perfusion can be characterized noninvasively by MRI, via application of DCE-MRI (34–37). The DCE data indicating higher permeability supports the histologic analysis of perfusion and the IFP data: 3 days following Cellax treatment, the tumor vessel permeability in the core of tumors (K_{trans}) was significantly increased compared with other therapies (Fig. 1F).

Neither native docetaxel or nab-paclitaxel treatments significantly altered α -SMA content in the 4T1 and MDA-MB-231 tumors, nor were there significant alterations to matrix or IFP. Native docetaxel treatment increased the number of lung metastases in the MDA-MB-231 model, suggesting that chemotherapy treatment could induce a more aggressive phenotype of tumor. Shaked and colleagues (38) observed that taxane therapy increased the production of SDF-1 and granulocyte colony-stimulating factor from host cells, factors that promoted tumor revascularization and progression. The plasma collected from the taxane-treated mice induced bone marrow-derived cells and tumors cells to release MMP-9, and enhanced the invasiveness and metastasis of the tumor cells. In addition, damage to tumor vasculature by chemotherapy or antivascular antibodies can lead to recruitment of

endothelial progenitor cells (EPC), promoting angiogenesis, leading to increased IFP and decreased permeability (12, 38, 39). These negative effects induced by standard taxanes were observed in our animal models, including decreased permeability and perfusion (4T1 model), and increased metastases (MDA-MB-231 model). In contrast, Cellax did not induce these effects.

We have reported that Cellax nanoparticles accumulate in tumors by the EPR effect, but these earlier studies did not identify which cell populations Cellax was interacting with in the tumor microenvironment (15, 17). The stroma-depleting activity of Cellax could be a primary (Cellax-targeted stroma) or secondary effect (Cellax induced toxicity in tumor cells first, resulting in deactivation of the stromal cells). To elucidate the mode of action of Cellax, we analyzed the intratumoral uptake and therapeutic impact of Cellax in α -SMA stroma and tumor cells separately. One day after an intravenous dose of fluorescently labeled Cellax (Cellax-DiI), the nanoparticles preferentially colocalized with α -SMA stromal cells (>85%) (Fig 5A). The kinetics of population decline of α -SMA and tumor cells in the 4T1 tumor agree with the intratumoral uptake data. As the majority of Cellax was taken up by α -SMA+ cells, the α -SMA content in the tumor rapidly decreased from approximately 30% to approximately 10% of the tumor area at 16 hours posttreatment, and then steadily declined to almost 0% in 1 week. The epithelial tumor cell population did not interact as significantly with Cellax nanoparticles, was not affected for the first 3 days of therapy, and the population only started to decline when the α -SMA was depleted on day 7 (Fig. 5B). The data suggest that α -SMA+ stroma is the primary target of Cellax, and the decline of the tumor cell population could be attributed to the residually released dose from Cellax nanoparticles or decreased paracrine survival signals from the stromal cells. The molecular mechanism for the interaction of Cellax with α -SMA+ stroma is under investigation. In preliminary studies, we have discovered that Cellax efficiently adsorbs serum albumin (0.5 μ g albumin/mg polymer), and the cellular internalization of Cellax is favored by SPARC+ (secreted protein acidic and rich in cysteine) cells, especially in the presence of albumin. Stromal cells (especially α SMA+ CAF) produce significantly elevated levels of SPARC: in nab-paclitaxel and now Cellax studies, there seems to be a stromal interaction due to the albumin-SPARC mechanism (40). We had previously observed toxicity effects arising from native docetaxel and nab-paclitaxel treatments in mice, with more than 50% reductions in neutrophils after 1 dose at their MTDs, and this effect was sustained over multiple doses (15, 16). Conversely, Cellax treatment was not observed to induce neutropenia. To further substantiate the safety profile of Cellax, we monitored mice for 4 weeks following 3 weekly cycles at the 170 mg docetaxel/kg level, scrutinizing for late presentation of toxicity upon multiple doses, given that Cellax is a long-circulating and slow releasing formulation. No abnormalities appeared in hematology or blood chemistry parameters during dosing or postdosing (all parameters were within normal limits for Balb/c mice; Fig. 6 and Supplementary Table S1). Pathologic analysis of liver tissues 1 week subsequent to the 3rd dose indicated hypertrophy in selected Kupffer cells (macrophages), an observation consistent with

the biodistribution of Cellax (15) and many other nanoparticle systems (41), in which the RES (reticuloendothelial system) is the major system of clearance. Kupffer cells are responsible for clearance of foreign particles, and are cells that are continuously replenished. Cellax accumulation to lung tissues was identified previously as insignificant (15). We tested the serum of mice treated with 170 mg docetaxel/kg Cellax for indicators of an inflammatory response using a Luminex assay for 23 inflammatory cytokines (Supplementary Fig S2), and detected no elevation of any cytokine. As the findings in the liver and lungs were minor and attenuated by 4 weeks, with no evidence of fibrosis, necrosis, blood vessel disruption, or organ malfunction, we conclude that organ responses at the 170 mg docetaxel/kg dose were within acceptable parameters.

In summary, we have shown that Cellax interacted substantially with tumor stroma and depleted this population in 2 orthotopic breast tumor models. Tumor stroma is an established prognostic marker for survival in women with breast cancer (9, 26), largely due to stromal influence on tumor survival and metastasis. In the 2 mouse models, Cellax treatment depleted stroma and inhibited matrix deposition, decreased tumor IFP, increased perfusion, and significantly suppressed lung metastases.

Disclosure of Potential Conflicts of Interest

No potential conflicts of interest were disclosed.

Authors' Contributions

Conception and design: M. Murakami, M.J. Ernsting, W. Foltz, S.D. Li
Development of methodology: M. Murakami, M.J. Ernsting, W. Foltz, S.D. Li
Acquisition of data (provided animals, acquired and managed patients, provided facilities, etc.): M. Murakami, M.J. Ernsting, E. Undzys, W. Foltz, S.D. Li
Analysis and interpretation of data (e.g., statistical analysis, biostatistics, computational analysis): M. Murakami, M.J. Ernsting, W. Foltz, S.D. Li
Writing, review, and/or revision of the manuscript: M. Murakami, M.J. Ernsting, W. Foltz, S.D. Li
Administrative, technical, or material support (i.e., reporting or organizing data, constructing databases): M. Murakami, M.J. Ernsting, E. Undzys, N. Holwell, S.D. Li
Study supervision: M. Murakami, M.J. Ernsting, S.D. Li

Acknowledgments

The authors thank Dr. Ian F Tannock, Dr. Herman Chung, and Dr. Jonathan May for reviewing the manuscript, Dr. Richard Hill at the University Health Network (Toronto) for the IFP analysis equipment, Trevor Do at the STTARR facility for Definiens analysis, Dr. Hibret Adissu at the Toronto Centre for Phenogenomics for pathology analysis, and the Nanotechnology Characterization Lab (US National Cancer Institute) for characterization of the Cellax nanoparticles.

Grant Support

This work was funded by grants from the Ontario Institute for Cancer Research Intellectual Property Development and Commercialization Fund, the Canadian Institutes of Health Research operating grant and proof-of-principal grant, MaRS Innovation and Ontario Centres of Excellence proof-of-principal grant, the National Cancer Institute Nanotechnology Characterization, and the Prostate Cancer Foundation. The Ontario Institute for Cancer Research is financially supported by the Ontario Ministry of Economic Development and Innovation.

The costs of publication of this article were defrayed in part by the payment of page charges. This article must therefore be hereby marked *advertisement* in accordance with 18 U.S.C. Section 1734 solely to indicate this fact.

Received January 10, 2013; revised March 25, 2013; accepted April 28, 2013; published online August 1, 2013.

References

- National Cancer Institute Bethesda, MD: NCI Breast Cancer; August 5, 2012. Available from: <http://www.cancergov/cancertopics/types/breast>.
- Jemal A, Siegel R, Xu J, Ward E. Cancer statistics, 2010. *CA Cancer J Clin* 2010;60:277–300.
- Weigelt B, Peterse JL, van 't Veer LJ. Breast cancer metastasis: markers and models. *Nat Rev Cancer* 2005;5:591–602.
- Fang J, Nakamura H, Maeda H. The EPR effect: Unique features of tumor blood vessels for drug delivery, factors involved, and limitations and augmentation of the effect. *Adv Drug Deliv Rev* 2011;63:136–51.
- Jain RK, Stylianopoulos T. Delivering nanomedicine to solid tumors. *Nat Rev Clin Oncol* 2010;7:653–64.
- Maeda H, Sawa T, Konno T. Mechanism of tumor-targeted delivery of macromolecular drugs, including the EPR effect in solid tumor and clinical overview of the prototype polymeric drug SMANCS. *J Control Release* 2001;74:47–61.
- Matsumura Y, Maeda H. A new concept for macromolecular therapeutics in cancer chemotherapy: mechanisms of tumoritropic accumulation of proteins and the antitumor agent smancs. *Cancer Res* 1986;46:6387–92.
- Li SD, Huang L. Pharmacokinetics and biodistribution of nanoparticles. *Mol Pharm* 2008;5:496–504.
- Mueller MM, Fusenig NE. Friends or foes—bipolar effects of the tumour stroma in cancer. *Nat Rev Cancer* 2004;4:839–49.
- Tarin D, Croft CB. Ultrastructural features of wound healing in mouse skin. *J Anat* 1969;105:189–90.
- Cirri P, Chiarugi P. Cancer associated fibroblasts: the dark side of the coin. *Am J Cancer Res* 2011;1:482–97.
- Eckhardt BL, Francis PA, Parker BS, Anderson RL. Strategies for the discovery and development of therapies for metastatic breast cancer. *Nat Rev Drug Discov* 2012;11:479–97.
- Neesse A, Michl P, Frese KK, Feig C, Cook N, Jacobetz MA, et al. Stromal biology and therapy in pancreatic cancer. *Gut* 2011;60:861–8.
- Ernsting MJ, Tang WL, Maccallum N, Li SD. Synthetic modification of carboxymethylcellulose and use thereof to prepare a nanoparticle forming conjugate of docetaxel for enhanced cytotoxicity against cancer cells. *Bioconjug Chem* 2011;22:2474–86.
- Ernsting MJ, Tang WL, Maccallum NW, Li SD. Preclinical pharmacokinetic, biodistribution, and anti-cancer efficacy studies of a docetaxel-carboxymethylcellulose nanoparticle in mouse models. *Biomaterials* 2012;33:1445–54.
- Ernsting MJ, Murakami M, Undyys E, Aman A, Press B, Li SD. A docetaxel-carboxymethylcellulose nanoparticle outperforms the approved taxane nanoformulation, Abraxane, in mouse tumor models with significant control of metastases. *J Control Release* 2012;162:575–81.
- Ernsting MJ, Foltz WD, Undyys E, Tagami T, Li SD. Tumor-targeted drug delivery using MR-contrasted docetaxel - Carboxymethylcellulose nanoparticles. *Biomaterials* 2012;33:3931–41.
- Milosevic M, Lunt SJ, Leung E, Skliarenko J, Shaw P, Fyles A, et al. Interstitial permeability and elasticity in human cervix cancer. *Microvasc Res* 2008;75:381–90.
- Skliarenko JV, Lunt SJ, Gordon ML, Vitkin A, Milosevic M, Hill RP. Effects of the vascular disrupting agent ZD6126 on interstitial fluid pressure and cell survival in tumors. *Cancer Res* 2006;66:2074–80.
- Chung C, Jalali S, Foltz W, Burrell K, Wildgoose P, Lindsay P, et al. Imaging biomarker dynamics in an intracranial murine glioma study of radiation and antiangiogenic therapy. *Int J Radiat Oncol Biol Phys* 2013;85:805–12.
- Tofts PS. Modeling tracer kinetics in dynamic Gd-DTPA MR imaging. *J Magn Reson Imaging* 1997;7:91–101.
- Kalluri R, Zeisberg M. Fibroblasts in cancer. *Nat Rev Cancer* 2006;6:392–401.
- Joyce JA, Pollard JW. Microenvironmental regulation of metastasis. *Nat Rev Cancer* 2009;9:239–52.
- Eckhardt BL, Parker BS, van Laar RK, Restall CM, Natoli AL, Tavaría MD, et al. Genomic analysis of a spontaneous model of breast cancer metastasis to bone reveals a role for the extracellular matrix. *Mol Cancer Res* 2005;3:1–13.
- Erkan M, Michalski CW, Rieder S, Reiser-Erkan C, Abiatari I, Kolb A, et al. The activated stroma index is a novel and independent prognostic marker in pancreatic ductal adenocarcinoma. *Clin Gastroenterol Hepatol* 2008;6:1155–61.
- Moorman AM, Vink R, Heijmans HJ, van der Palen J, Kouwenhoven EA. The prognostic value of tumour-stroma ratio in triple-negative breast cancer. *Eur J Surg Oncol* 2012;38:307–13.
- de Kruijf EM, van Nes JG, van de Velde CJ, Putter H, Smit VT, Liefers GJ, et al. Tumor-stroma ratio in the primary tumor is a prognostic factor in early breast cancer patients, especially in triple-negative carcinoma patients. *Breast Cancer Res Treat* 2011;125:687–96.
- Minn AJ, Gupta GP, Sigel PM, Bos PD, Shu W, Giri DD, et al. Genes that mediate breast cancer metastasis to lung. *Nature* 2005;436:518–24.
- Jain RK, Tong RT, Munn LL. Effect of vascular normalization by antiangiogenic therapy on interstitial hypertension, peritumor edema, and lymphatic metastasis: insights from a mathematical model. *Cancer Res* 2007;67:2729–35.
- Netti PA, Hamberg LM, Babich JW, Kierstead D, Graham W, Hunter GJ, et al. Enhancement of fluid filtration across tumor vessels: implication for delivery of macromolecules. *Proc Natl Acad Sci U S A* 1999;96:3137–42.
- Olive KP, Jacobetz MA, Davidson CJ, Gopinathan A, McIntyre D, Honess D, et al. Inhibition of Hedgehog signaling enhances delivery of chemotherapy in a mouse model of pancreatic cancer. *Science* 2009;324:1457–61.
- Hori K, Saito S. Microvascular mechanisms by which the combretastatin A-4 derivative AC7700 (AVE8062) induces tumour blood flow stasis. *Br J Cancer* 2003;89:1334–44.
- Beauregard DA, Hill SA, Chaplin DJ, Brindle KM. The susceptibility of tumors to the antivascular drug combretastatin A4 phosphate correlates with vascular permeability. *Cancer Res* 2001;61:6811–5.
- Aoyagi T, Shuto K, Okazumi S, Hayano K, Satoh A, Saitoh H, et al. Apparent diffusion coefficient correlation with oesophageal tumour stroma and angiogenesis. *Eur Radiol* 2012;22:1172–7.
- Li W, Zhang Z, Nicolai J, Yang GY, Omary RA, Larson AC. Magnetization transfer MRI in pancreatic cancer xenograft models. *Magn Reson Med* 2012;68:1291–7.
- Muraoka N, Uematsu H, Kimura H, Imamura Y, Fujiwara Y, Murakami M, et al. Apparent diffusion coefficient in pancreatic cancer: characterization and histopathological correlations. *J Magn Reson Imaging* 2008;27:1302–8.
- Wang Y, Chen ZE, Nikolaidis P, McCarthy RJ, Merrick L, Sternick LA, et al. Diffusion-weighted magnetic resonance imaging of pancreatic adenocarcinomas: association with histopathology and tumor grade. *J Magn Reson Imaging* 2011;33:136–42.
- Gingis-Velitski S, Loven D, Benayoun L, Munster M, Bril R, Voloshin T, et al. Host response to short-term, single-agent chemotherapy induces matrix metalloproteinase-9 expression and accelerates metastasis in mice. *Cancer Res* 2011;71:6986–96.
- Shaked Y, Henke E, Roodhart JM, Mancuso P, Langenberg MH, Colleoni M, et al. Rapid chemotherapy-induced acute endothelial progenitor cell mobilization: implications for antiangiogenic drugs as chemosensitizing agents. *Cancer Cell* 2008;14:263–73.
- Von Hoff DD, Ramanathan RK, Borad MJ, Laheru DA, Smith LS, Wood TE, et al. Gemcitabine plus nab-paclitaxel is an active regimen in patients with advanced pancreatic cancer: a phase I/II trial. *J Clin Oncol* 2011;29:4548–54.
- Greish K, Thiagarajan G, Ghandehari H. *In vivo* methods of nanotoxicology. *Methods Mol Biol* 2012;926:235–53.